Cases from a busy nuclear cardiology laboratory

Andrew A. Girard, MD,[a] Jacob Elrod, MD,[b] Pradeep Bhambhvani, MD,[c] and Fadi G. Hage, MD[b,d]

[a] Department of Medicine, The University of Alabama at Birmingham, Birmingham, AL
[b] Division of Cardiovascular Disease, Department of Medicine, The University of Alabama at Birmingham, Birmingham, AL
[c] Division of Molecular Imaging and Therapeutics, Department of Radiology, The University of Alabama at Birmingham, Birmingham, AL
[d] Section of Cardiology, Birmingham Veterans Affairs Medical Center, Birmingham, AL

Received Sep 9, 2022; accepted Sep 14, 2022
doi:10.1007/s12350-022-03114-1

CASE 1

A 67-year-old woman with chronic low back pain and active tobacco use presents for a preoperative stress test for an abdominal aortic aneurysm repair. Her ability to exercise is limited by back pain. She denies any chest pain or shortness of breath at rest or with limited exertion. Physical examination is unremarkable with a blood pressure of 145/82 mm Hg, heart rate of 75 beats per minute (bpm), and oxygen saturation of 95% on room air.

Regadenoson Single-Photon Emission Computed Tomography (SPECT) Myocardial Perfusion Imaging (MPI) using a GE Discovery 530 CZT camera demonstrated normal perfusion (Figure 1A). Review of the simulated rotating planar projection images was not revealing, but inspection of the individual planar projections demonstrated focal radiotracer uptake in the superior left thorax (Figure 1B).

A follow-up computed tomography (CT) scan of the chest with contrast revealed the presence of a 11 × 12 mm spiculated nodule in the left upper lobe of the lung. A fluorodeoxyglucose positron emission tomography (FDG-PET) scan confirmed avid FDG uptake (maximum standard uptake value [SUV] = 10) without evidence of nodal metastasis (Figure 1C). She underwent an endobronchial ultrasound with biopsy, confirming the diagnosis of poorly differentiated adenocarcinoma of the lung. She is currently awaiting a left upper lobectomy with thoracic surgery.

Teaching points

Nuclear stress imaging relies on the capture of gamma rays emitted from a decaying radiotracer. This is achieved using a detector (scintillator) mounted on a rotating or fixed gantry. In SPECT MPI, traditional Anger cameras rotate the detectors around the patient using a gantry to generate the image and therefore does not differentiate between cardiac and extra-cardiac structures. Dedicated cardiac cameras, such as the one used to image this patient, use advances in detector and collimator technologies to focus the image on the heart. This results in substantial improvement in sensitivity of detecting gamma rays emitted from the myocardium, and ultimately enhancement of spatial resolution in the cardiac region.[1,2] However, this comes at the expense of reduced count sensitivity and resolution in the surrounding extra-cardiac regions. The estimated prevalence and distribution of incidental extra-cardiac findings (IECFs) seen during SPECT and PET MPI have been documented.[3–5] It is essential that the interpreting physician examine all structures both within and outside of the myocardium during review of images since IECFs may be clinically important. For SPECT imaging, this entails visualizing the raw projection images. With the conventional Anger camera, inspection of the endless-loop cine of the raw data allows for visualizing IECFs adequately either as increased or decreased tracer uptake. With cardiac-focused cameras, the simulated rotating image may not show significant IECFs, as demonstrated in this case. The interpreting physician should routinely review the individual raw planar projections for IECFs on these cameras.

This case does not include any PHI and is exempt from an IRB protocol at this institution.

Funding None.

Reprint requests: Andrew A. Girard, MD, Department of Medicine, The University of Alabama at Birmingham, 1720 2nd Ave S, BDB 327, Birmingham, AL 35233; *aagirard@uabmc.edu*

J Nucl Cardiol
1071-3581/$34.00

Published online: 07 October 2022

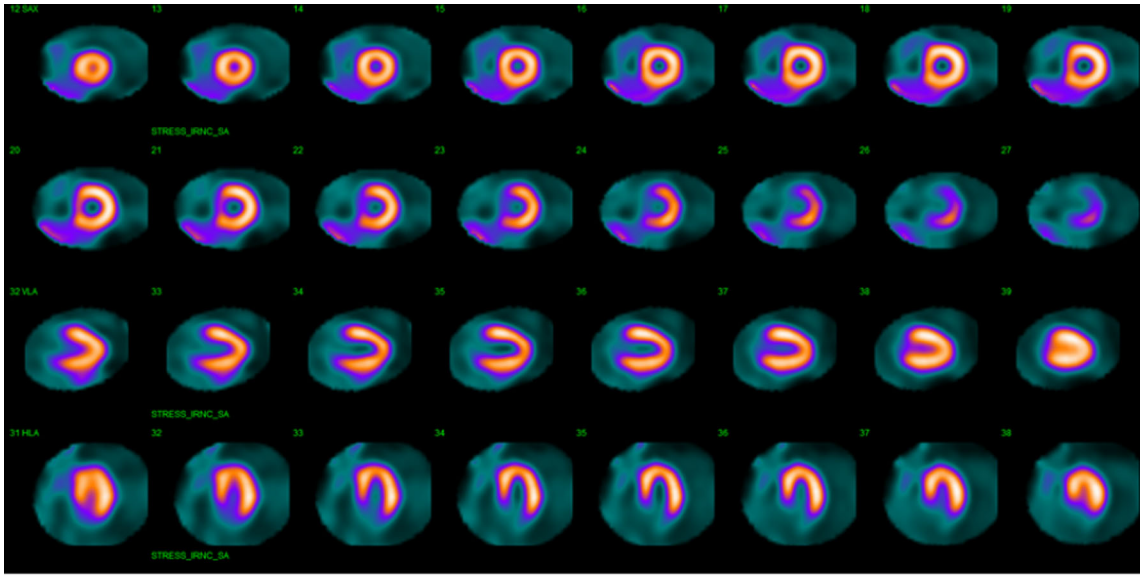

A

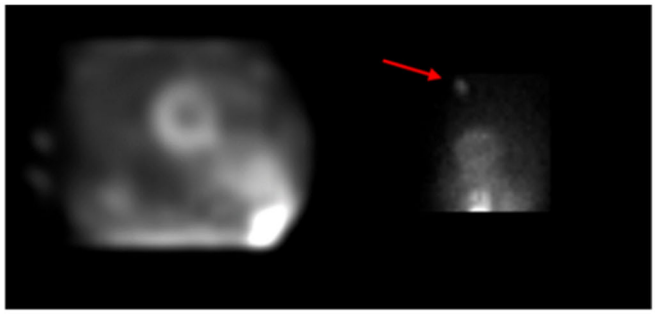

B

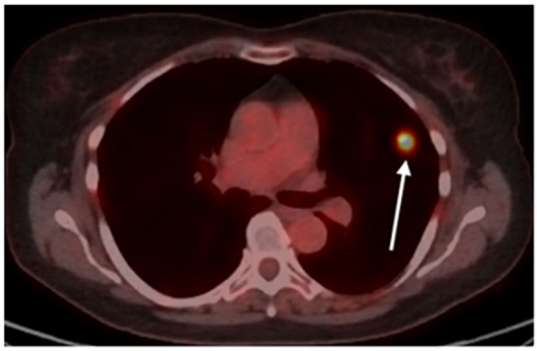

C

Figure 1. A Regadenoson SPECT MPI study demonstrating homogenous uptake of radiotracer throughout the left ventricular myocardium. **B** Right image: One of the 19 raw projection images revealed significant focal radiotracer uptake in the superior left thorax (red arrow). Left image: The simulated rotating planar projection image did not reproduce this finding. **C** FDG-PET scan revealed a hypermetabolic nodule (white arrow) in the superior left upper lobe of the lung which was determined to be poorly differentiated adenocarcinoma on biopsy.

CASE 2

A 59-year-old woman with coronary artery disease, peripheral vascular disease, severe chronic obstructive pulmonary disease on home oxygen, and a 50 pack-year history of tobacco use presented to the clinic for episodes of substernal chest pain that have been increasing in frequency and severity over the last year. Physical examination was unremarkable with a heart rate of 92 bpm, blood pressure of 132/59 mm Hg, and an oxygen saturation of 98% on 2 L of oxygen by nasal cannula. She was referred for a pharmacologic nuclear stress test.

Regadenoson SPECT MPI study with Technetium-99 m (Tc-99 m) showed normal perfusion. The simulated rotating planar projection images did not show any IECFs but a single raw planar projection showed focal radiotracer uptake located in the superior right thorax (Figure 2A). Review of rotating cine images obtained on an Anger camera 3 years prior did not show radiotracer uptake in the right lung at that time (Figure 2C). A CT scan confirmed the presence of a right apical lung nodule measuring approximately 7 × 10 mm with avid FDG uptake (maximum SUV = 4.2) on PET scan without evidence of nodal metastasis (Figure 2B).

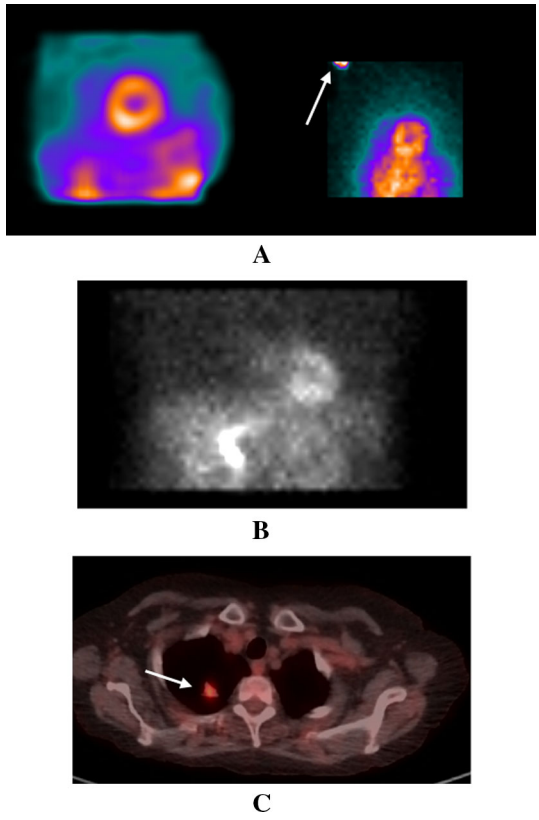

Figure 2. A Left panel: The simulated rotating projection image did not demonstrate an IECF. Right panel: A single raw projection planar image revealed focal radiotracer uptake (white arrow) in superior right thorax. **B** Cine rotating planar projection image on an Anger camera obtained 3 years prior did not show radiotracer uptake in that region. **C** FDG-PET scan showed a hypermetabolic nodule (SUV = 4.2) in the right lung apex without evidence of nodal metastasis.

Teaching points

Solitary pulmonary nodule is a common IECF, typically discovered on a chest x-ray or CT scan. The risk of malignancy associated with a lung nodule (or nodules) is determined by assessing patient characteristics and nodule size, appearance, and count.[6] Guidelines for the management of lung nodules are defined by the Fleischner Society.[7] A solitary, spiculated pulmonary nodule measuring > 8 mm with the patient characteristics described in this case is considered high risk and requires either surveillance CT scans every 3 months, PET/CT imaging, or tissue sampling. In this case, the spiculated lung nodule had notable radiotracer uptake on both a SPECT MPI study and an FDG-PET scan. Similar to the prior case, the simulated rotating planar projection images did not reveal radiotracer uptake. Focal radiotracer uptake was only seen when the single planar projections were reviewed.

CASE 3

A 52-year-old man with end stage kidney disease (ESKD), due to focal segmental glomerulosclerosis, presents to clinic for a third kidney transplantation evaluation. He initially received a living donor kidney transplant in 1995. He developed severe allograft rejection the following year which required intermittent hemodialysis until he received a second transplant in 2000. Since that time, he had been on stable immunosuppressive therapy. However, over the last two years he experienced a progressive decline in renal function to stage four chronic kidney disease. Two months ago, he was hospitalized for COVID-19 infection and acute kidney injury. As a result, he has progressed to ESKD, and is currently undergoing peritoneal dialysis pending identification of a suitable kidney transplant donor. He was referred for nuclear stress testing as a part of his transplantation evaluation.

Regadenoson SPECT MPI demonstrated normal perfusion. The simulated raw rotating planar projection images did not show any IECF (Figure 3A, right panel). However, focal radiotracer uptake was noted in the region of the thyroid and parathyroid glands on the planar projection images (Figure 3A, left panel). Thyroid function tests were normal. Parathyroid hormone (PTH) level was found to be elevated at 167.3 pg/mL

with a calcium level of 9.3 mg/dL and a phosphorous level of 7.0 mg/dL. A Sestamibi parathyroid scan identified multigland parathyroid hyperplasia (Figure 3B).

Teaching points

Nuclear stress testing is typically performed as part of the pre-renal transplantation evaluation.[8] Review of the raw planar projection images allowed for the identification of Tc-99m uptake in the region of the thyroid and parathyroid gland in this patient. Previous reports documenting the incidental findings of parathyroid uptake following SPECT MPI have also emphasized the importance of reviewing the raw planar projection data.[9,10] The presence of uptake in this region should prompt biochemical evaluation for thyroid and parathyroid abnormalities. In the case of hyperparathyroidism, elevated calcium and PTH levels are diagnostic. When primary hyperparathyroidism is suspected, preoperative Tc-99m Sestamibi planar and SPECT scintigraphy can demonstrate the location of an abnormal gland and help guide the necessary operative intervention.[11] Secondary hyperparathyroidism can result from vitamin D deficiency or, as in this patient, from ESKD. In cases of secondary hyperparathyroidism resulting from ESKD, initial management includes phosphate binders for phosphate levels persistently > 5.5 mg/dL, vitamin D for patients with vitamin D deficiency or severe hypocalcemia, and calcitriol for persistently elevated (150 to 200 pg/mL) or rising PTH levels. Ultimately, kidney transplantation is required for definitive correction of mineral bone disease and secondary hyperparathyroidism associated with ESKD.

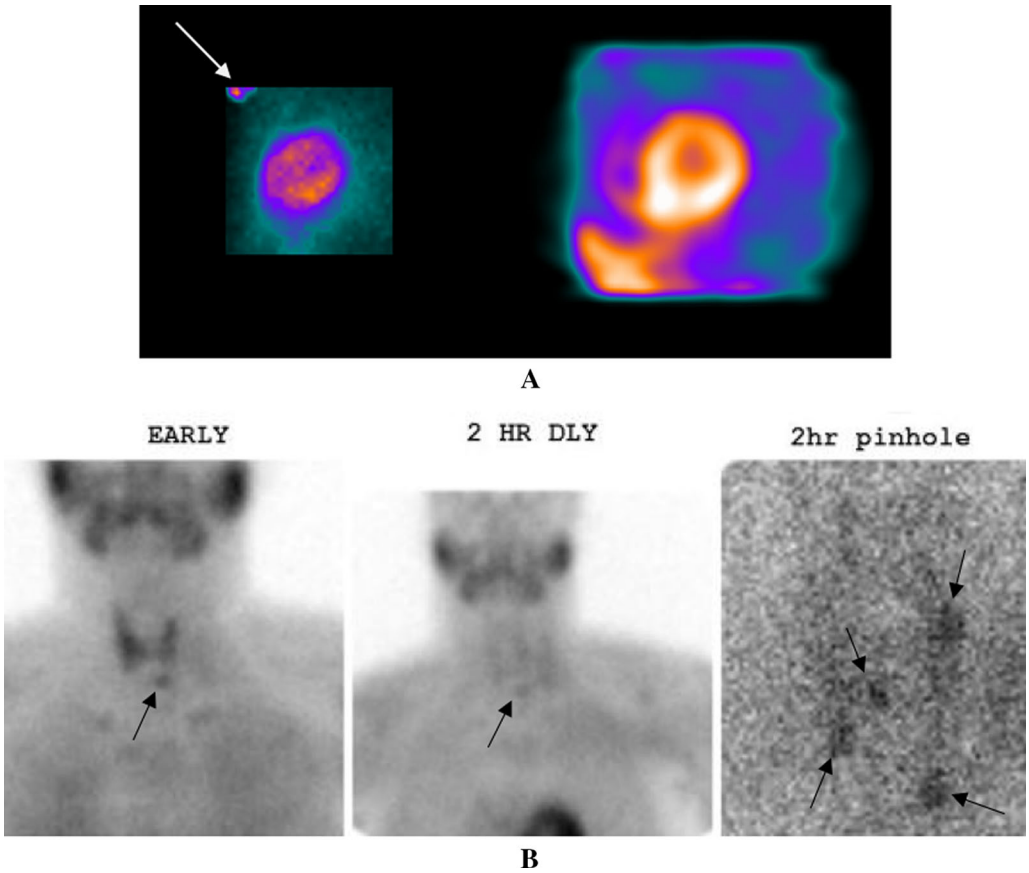

Figure 3. A Right panel: The simulated rotating planar projection images showed no IECF. Left panel: A raw projection planar image revealed significant radiotracer uptake in the regions of the thyroid and parathyroid glands (white arrow). The exact location of radiotracer uptake is difficult to discern, necessitating biochemical evaluation of thyroid and parathyroid function. **B**. Early, 2 h delayed, and 2 h delayed pinhole magnified Sestamibi parathyroid images show multigland parathyroid hyperplasia (black arrows).

CASE 4

A 73-year-old woman with chronic kidney disease stage 3, atrial fibrillation, and hypertension is currently being evaluated for a neck mass which has gradually increased in size over the past 3 months. She has also experienced worsening dysphagia to both solids and liquids as well as hoarseness. An ultrasound of the neck obtained one month ago revealed the presence of a left thyroid lobe mass extending caudally into the upper mediastinum and laterally into the neck with infiltration of the left sternocleidomastoid muscle. The mass also partially encases the left common carotid artery and left internal jugular vein. Fine needle aspiration of the mass was performed, and the histologic specimen was classified as Bethesda 6 (malignant). She was referred to our institution for further evaluation of the neck mass.

A CT with contrast of the chest showed a 6.6 × 5.3 cm mass originating from the left lobe of the thyroid gland (Figure 4A) with extension into the mediastinum. Multiple bilateral lung nodules measuring 4–14 mm were also seen. An open thyroid biopsy later confirmed the diagnosis of anaplastic thyroid carcinoma. The patient underwent a staging whole-body FDG-PET. Notable cardiac findings included a hypermetabolic pericardiophrenic lymph node, cardiomegaly, coronary atherosclerosis, and marked focal uptake (maximum SUV = 21.4) in the right atrium (Figure 4B). Extracardiac findings included focal uptake within multiple lung nodules, as well as multiple hypermetabolic lymph nodes located in the hilum of lung, mediastinum, and abdomen. Abnormal uptake was also noted within the soft tissues of bilateral hips and left posterior fourth rib. Given the advanced stage of the thyroid carcinoma (stage IV), she elected to undergo palliative radiation therapy for the neck mass.

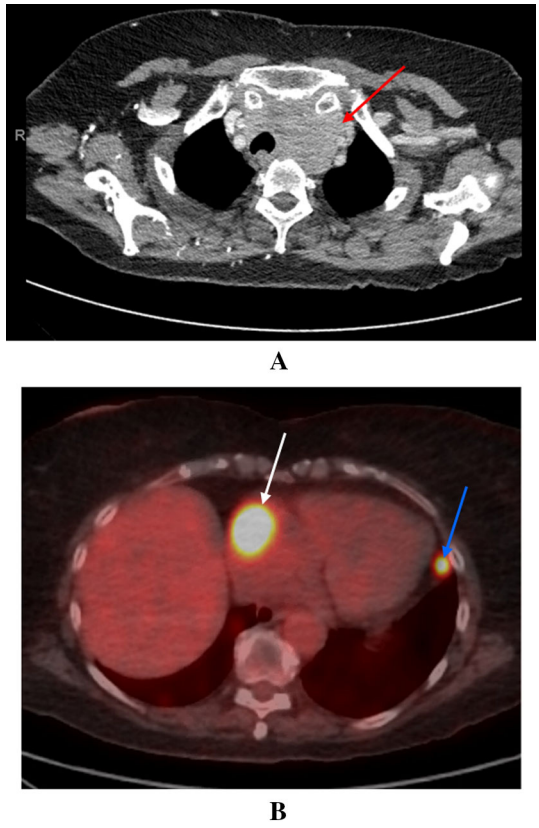

Figure 4. **A** CT scan of the chest with contrast, at the level of the neck. Imaging demonstrates the presence of a 6.6 × 5.3 cm mass (red arrow) originating from the left lobe of the thyroid gland. There is extension of the mass into the superior mediastinum. **B.** FDG-PET scan with a four-chamber cardiac view. Notable cardiac findings seen in this view included a hypermetabolic pericardiophrenic lymph node (blue arrow) and a right atrial metastatic lesion (white arrow).

Teaching points

FDG-PET imaging can be used to detect metabolically active lesions during oncologic evaluation. The cardio-oncologic findings seen on PET imaging in this case were notable for a hypermetabolic pericardiophrenic lymph node and a large right atrial metastatic lesion. The classification of cardiac neoplasms includes primary or secondary tumors (metastases). Generally, cardiac metastases are far more common than primary cardiac tumors and indicate the presence of an advanced stage or aggressive extra-cardiac neoplasm.[12] Clinically, cardiac metastases usually present without symptoms, but may occasionally cause dyspnea or chest pain.[13] Therefore, it is plausible that this patient could have initially presented following a PET scan for a cardiovascular indication. In such a case, a thorough evaluation of all PET scan slices is warranted to detect the presence of cardiac and extracardiac metastases. However, it should be noted that PET scans performed for cardiac indications are typically limited to the thoracic cavity and repeat imaging with a whole-body scan is warranted.

CASE 5

A 73-year-old woman with a history of presumed chronic pulmonary thromboembolism presents to our institution as a transfer from an outside hospital for hemoptysis and acute hypoxemic respiratory failure requiring intubation. One year prior to this admission, the patient underwent a CT angiogram for shortness of breath following a drive from Alabama to Texas. It revealed a pulmonary embolus completely filling and obstructing the right main pulmonary artery. During the past year, she was treated with multiple direct oral

anticoagulants, but all were discontinued due to an increasing clot burden. More recently, warfarin was initiated for anticoagulation, but the patient has continued to worsen from a respiratory standpoint.

Her vital signs were notable for a blood pressure of 124/59 mmHg, heart rate of 57 bpm, temperature of 98.4 F, and oxygen saturation of 100% on 40% oxygen with mechanical ventilation. A repeat CT angiogram of the chest revealed a thromboembolus occluding the main pulmonary artery with extension into the segmental and subsegmental vessels of the right lung (Fig. 5A–B). Pulmonary infarcts were also present in the periphery of the right lung. The clot further extended into the right ventricular outflow tract (RVOT). A transthoracic echocardiogram did not show evidence of right ventricular dysfunction but was notable for a right ventricular systolic pressure of 61 mm Hg. Bilateral lower extremity ultrasound was negative for deep vein thrombosis.

Given the expanding size of the RVOT mass in the setting of adequate anticoagulation, an angiosarcoma of the pulmonary artery was suspected. FDG-PET scan revealed the presence of hypermetabolic intravascular mass (maximum SUV = 11.27 in the right ventricle) seen throughout the right pulmonary vasculature beginning at the RVOT and extending through the main pulmonary artery to the right upper, middle, and lower lobar arteries (Figure 5C). A mix of metabolically inactive and active thrombi were also seen in the main pulmonary artery, depicted by the black and red arrows within Figure 5C. No hypermetabolic metastatic lesions were seen. Incidental post pleurodesis inflammatory uptake was also noted (blue arrows Figure 3C). The patient subsequently underwent a pulmonary angiogram with biopsy of the mass. Pathology results were notable for a spindle cell angiosarcoma involving the RVOT.

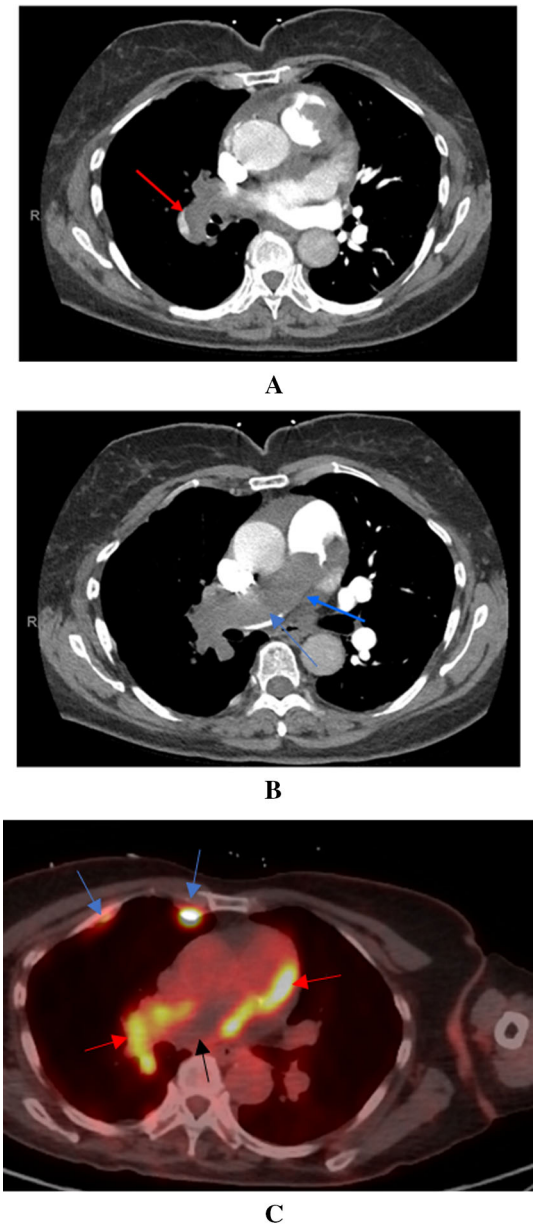

Figure 5. **A** CT pulmonary angiogram at the level of the right main pulmonary artery. There is extension of the mass into the right segmental pulmonary artery (red arrow). **B** CT pulmonary angiogram at the level of the main pulmonary artery. The mass extends completely through the main pulmonary artery (blue arrow). **C** FDG-PET scan revealing the presence of a hypermetabolic tumor thrombus (red arrows) and hypometabolic bland thrombus (black arrow) in the main and right pulmonary arteries. Post right-sided pleurodesis inflammatory plaques are incidentally seen (blue arrows).

Teaching points

Angiosarcomas involving the RVOT are associated with an extremely poor prognosis due to their aggressive nature.[14,15] Because angiosarcomas can involve the right side of the heart or RVOT, presenting symptoms commonly include dyspnea and chest discomfort.[16] At the time of diagnosis, metastases are typically present and often involve the lung.[14,16] Angiosarcomas rapidly progress and culminate in death within weeks to months because of hemodynamic compromise (e.g., valvular obstruction), local invasion, or metastatic spread. Thus, early diagnosis is essential.

Cardiac angiosarcomas pose a particular diagnostic challenge as their appearance on imaging can mimic pulmonary emboli.[17] Thus, conventional imaging with transesophageal echocardiography, CT, and cardiac magnetic resonance imaging with gadolinium contrast are of little utility in distinguishing malignant from non-malignant lesions. However, FDG-PET has shown potential in differentiating benign from malignant

disease.[18,19] In a recent study involving 38 patients undergoing FDG-PET with malignant primary cardiac neoplasms, the majority of which were cardiac angiosarcomas, a maximum SUV at a minimum threshold of 3.44 provided a 100% sensitivity and 92% specificity for the detection of malignant neoplasms.[20] Tissue biopsy ultimately provides definitive diagnosis. Treatment is complete resection, often with neoadjuvant and postoperative chemotherapy.

Author contributions

All authors had full access to the data when designing and drafting the manuscript.

Disclosures

All authors have no disclosures in relation to this manuscript.

References

1. Hawman PC, Haines EJ. The cardiofocal collimator: A variable-focus collimator for cardiac SPECT. Phys Med Biol 1994;39:439-50.
2. Dorbala S, Ananthasubramaniam K, Armstrong IS, Chareonthaitawee P, DePuey EG, Einstein AJ. Single photon emission computed tomography (SPECT) myocardial perfusion imaging guidelines: Instrumentation, acquisition, processing, and interpretation. J Nucl Cardiol 2018;25:1784-846.
3. Williams KA, Hill KA, Sheridan CM. Noncardiac findings on dual-isotope myocardial perfusion SPECT. J Nucl Cardiol 2003;10:395-402.
4. Kan H, van der Zant FM, Wondergem M, Knol RJJ. Incidental extra-cardiac findings on 13N-ammonia myocardial perfusion PET/CT. J Nucl Cardiol 2017;24:1860-8.
5. Saab R, Farag A, White S, Hage FG, Bhambhvani P. Artifacts and Incidental Findings on Myocardial Perfusion Imaging. In: Hage FG (ed) Myocardial Perfusion Imaging (MPI): Performance, Potential Risks and Outcomes. Nova Science Publishers. 2018. ISBN: 978-1-53613-476-6.
6. McWilliams A, Tammemagi MC, Mayo JR, Roberts H, Liu G, Soghrati K, et al. Probability of cancer in pulmonary nodules detected on first screening CT. N Engl J Med 2013;369:910-9.
7. MacMahon H, Naidich DP, Goo JM, Lee KS, Leung ANC, Mayo JR, et al. Guidelines for management of incidental pulmonary nodules detected on CT images: from the Fleischner Society 2017. Radiology 2017;284:228-43.
8. Ives CW, AlJaroudi WA, Kumar V, Farag A, Rizk DV, Oparil S, et al. Prognostic value of myocardial perfusion imaging performed pre-renal transplantation: post-transplantation follow-up and outcomes. Eur J Nucl Med Mol Imaging 2018;45:1998-2008.
9. Iagaru A, Hachamovitch R, Colletti PM, Wassef H. Demonstration of an ectopic mediastinal parathyroid adenoma on Tc-99m sestamibi myocardial perfusion scintigraphy. J Nucl Cardiol 2006;13:719-21.
10. Chamarthy M, Travin MI. Altered biodistribution and incidental findings on myocardial perfusion imaging. Semin Nucl Med 2010;40:257-70.
11. Wilhelm SM, Wang TS, Ruan DT, Lee JA, Asa SL, Duh QY, et al. The American association of endocrine surgeons guidelines for definitive management of primary hyperparathyroidism. JAMA Surg 2016;151:959-68.
12. Butany J, Leong SW, Carmichael K, Komeda M. A 30-year analysis of cardiac neoplasms at autopsy. Can J Cardiol 2005;21:675-80.
13. Yusuf SW, Bathina JD, Qureshi S, Kaynak HE, Banchs J, Trent JC, et al. Cardiac tumors in a tertiary care cancer hospital: clinical features, echocardiographic findings, treatment and outcomes. Heart Int 2012;7:e4.
14. Omair M, Calafiore P, Lim R, McGiffin D, Farouque O, Jones E. Primary angiosarcoma-a rare cause of right ventricular outflow tract obstruction: case report and literature review. CASE 2019;3:284-7.
15. Hohmann C, Pfister R, Ney S, Fink L, Bunck AC, Michels G. Pulmonary angiosarcoma: a rare cause of right ventricular outflow tract obstruction. J Cardiovasc Med 2021;22:664-7.
16. Ge Y, Ro JY, Kim D, Kim CH, Reardon MJ, Blackmon S, et al. Clinicopathologic and immunohistochemical characteristics of adult primary cardiac angiosarcomas: analysis of 10 cases. Ann Diagn Pathol 2011;15:262-7.
17. Ananthasubramaniam K, Farha A. Primary right atrial angiosarcoma mimicking acute pericarditis, pulmonary embolism, and tricuspid stenosis. Heart 1999;81:556-8.
18. Dhull VS, Sharma P, Mukherjee A, Jana M, Bal C, Kumar R. 18F-FDG PET-CT for evaluation of cardiac angiosarcoma: a case report and review of literature. Mol Imaging Radionucl Ther 2015;24:32-6.
19. Shao D, Wang SX, Liang CH, Gao Q. Differentiation of malignant from benign heart and pericardial lesions using positron emission tomography and computed tomography. J Nucl Cardiol 2011;18:668-77.
20. Meng J, Zhao H, Liu Y, Chen D, Hacker M, Wei Y, et al. Assessment of cardiac tumors by 18F-FDG PET/CT imaging: Histological correlation and clinical outcomes. J Nucl Cardiol 2021;28:2233-43.